catalysts

MDPI

Article

Kinetic Characterization of Pt/Al_2O_3 Catalyst for Hydrogen Production via Methanol Aqueous-Phase Reforming

José Sousa [1,2,3], Paranjeet Lakhtaria [1,2], Paulo Ribeirinha [1,2], Werneri Huhtinen [4], Johan Tallgren [4] and Adélio Mendes [1,2,*]

1 LEPABE—Laboratory for Process Engineering, Environment, Biotechnology and Energy, Faculty of Engineering, University of Porto, Rua Dr. Roberto Frias, 4200-465 Porto, Portugal; jmsousa@fe.up.pt (J.S.)
2 ALiCE—Associate Laboratory in Chemical Engineering, Faculty of Engineering, University of Porto, Rua Dr. Roberto Frias, 4200-465 Porto, Portugal
3 Departamento de Química, Escola de Ciências da Vida e do Ambiente, Universidade de Trás-os-Montes e Alto Douro, Quinta de Prados, 5000-801 Vila Real, Portugal
4 VTT Technical Research Centre of Finland Ltd., Tietotie 4 C, P.O. Box 1000, FI-02044 VTT Espoo, Finland
* Correspondence: mendes@fe.up.pt

Abstract: Compared to steam reforming, methanol aqueous-phase reforming (APR) converts methanol to hydrogen and carbon dioxide at lower temperatures, but also displays lower conversion rates. Herein, methanol APR is studied over the active Pt/Al_2O_3 catalyst under different operating conditions. Studies were conducted at different temperatures, pressures, methanol mass fractions, and residence times. APR performance was evaluated in terms of methanol conversion, hydrogen production rate, hydrogen selectivity, and by-product formation. The results revealed that an increase in operating pressure and methanol mass fraction had an adverse effect on the APR performance. Conversely, it was found that hydrogen selectivity was unaffected by the operating pressure and residence time for the methanol feed mass fraction of 5%. For the methanol feed mass fraction of 55%, hydrogen selectivity was improved by operating pressure and residence time. The alumina support phase change to boehmite as well as sintering and leaching of the catalytic particles were observed during catalyst stability experiments. Additionally, a comparison between methanol steam reforming (MSR) and APR was also performed.

Keywords: aqueous-phase reforming; methanol; catalyst; hydrogen production; Pt/Al_2O_3

Citation: Sousa, J.; Lakhtaria, P.; Ribeirinha, P.; Huhtinen, W.; Tallgren, J.; Mendes, A. Kinetic Characterization of Pt/Al_2O_3 Catalyst for Hydrogen Production via Methanol Aqueous-Phase Reforming. *Catalysts* **2024**, *14*, 741. https://doi.org/10.3390/catal14100741

Academic Editors: Georgios Bampos, Paraskevi Panagiotopoulou and Eleni A. Kyriakidou

Received: 19 August 2024
Revised: 14 October 2024
Accepted: 15 October 2024
Published: 21 October 2024

1. Introduction

Climate change, greenhouse gas emission, and the energy crisis have recently become major global concerns. The integration of carbon-neutral technologies, renewable energy resources, and reducing the usage of fossil fuels have become a priority [1,2]. For this energy transition, hydrogen has received a lot of attention, interest, and commitment from both the industrial and academic sectors. Hydrogen has been pushed forward for energy decarbonization, to mitigate the energy crisis pressed by geo-political conflicts, and to reach the "Paris agreement" [3,4].

The advantages of hydrogen are linked to its usability in a wide range of applications. For instance, hydrogen can be used directly as a fuel or as a raw material for the production of synthetic fuels and organic substances [5]. Yet, the main issues related to the use of hydrogen are related to its safe and efficient transportation and storage [6]. Even though the gravimetric energy density of hydrogen is excellent, the volumetric density is too low [5]. Hence, in situ hydrogen production has been suggested as an attractive approach, especially for systems with a demand for continuous hydrogen supply.

For in situ hydrogen production, there are different technologies, such as reforming and electrolysis [7,8]. Today, 96% of the world's hydrogen is still produced from fossil fuels, namely natural gas and coal [8,9]. To improve the sustainability of hydrogen production, interest

has been focused on the development of more environmentally friendly technologies. Apart from electrolysis, one interesting pathway is the use of renewable liquid fuels as feedstock for hydrogen production [10,11]. Biomass-derived organic waste streams containing alcohols have been investigated as potential bio-based feedstocks [12,13]. Compared to hydrogen, oxygenated hydrocarbons have a higher boiling point and, hence, have higher gravimetric density and are easier to transport and store [14]. In addition to its environmental merits, converting waste streams to value-added products is economically efficient.

There already exist mature reforming technologies of oxygenated hydrocarbons, such as the steam reforming of methanol (MSR) or ethanol [12,15]. The challenges with these technologies are related to the selectivity of the reaction, mainly to avoid the production of CO, in addition to the high amounts of energy necessary for vaporizing the reactants. The aqueous-phase reforming (APR) emerged then to address these challenges as a simpler and more energy-efficient technology [16,17]. The APR allows for converting the feeding fuel to hydrogen and CO_2 in a single-step catalytic process at temperatures lower than the well-established MSR. In APR, reactants are in the liquid phase and the reaction products are in the gas phase [18,19].

The APR of oxygenated hydrocarbons is often performed in a temperature range of 200–250 °C. To improve the overall efficiency of the APR system, the use of waste heat from other processes would be beneficial. The APR system should work with pressures above the bubble point pressure of the feedstock mixture to keep it in the aqueous phase. Bubble point pressure depends on the composition of the feedstock mixture and the selected operating temperature. In general, the working pressure should be between 1.5 and 5.0 MPa [14].

Mainly heterogeneous catalysts have been considered for the APR of oxygenated hydrocarbons [20]. Three phases exist in APR systems: solid (the catalyst), liquid (the feedstock), and gas (the evolved hydrogen and CO_2). This leads to mass transfer limitations, since the evolving gas bubbles may block the active sites of catalysts and decrease the hydrogen production rate [21]. To improve the reaction rate, it has been proposed to use an inert sweeping gas. The sweeping gas drives the evolved gas bubbles of hydrogen and CO_2 out of the catalyst active sites, improving the reaction performance of the APR [13,22].

Methanol has been used as a model compound in APR studies due to the absence of strong C-C bonds [22]. Methanol is a common by-product of chemical and biochemical processes and it has been pointed out as a very attractive green energy vector, which makes it cheap and readily available [23]. The overall APR reaction equation is given below, Equation (1):

$$CH_3OH\ (l) + H_2O\ (l) \rightleftharpoons 3\ H_2\ (g) + CO_2\ (g) \quad (1)$$

The methanol APR is based on two main reactions [24]: methanol dehydrogenation [Equation (2)] and WGS reaction [Equation (3)]. In the methanol dehydrogenation reaction, a methoxy intermediate is formed due to the split of the O-H bond of methanol [22]. Next, hydrogen atoms bonded to carbon in the methoxy intermediate are activated, which causes the decomposition of methoxy into hydrogen and carbon monoxide. Methanol dehydrogenation is followed by WGS, in which cleavage of O-H bonds of water leads to the formation of O^{2-} ion and hydrogen. Extremely active O^{2-} ion reacts with carbon monoxide forming carbon dioxide [22].

$$CH_3OH\ (l) \rightleftharpoons 2\ H_2\ (g) + CO\ (g) \quad (2)$$

$$CO\ (g) + H_2O\ (l) \rightleftharpoons H_2\ (g) + CO_2\ (g) \quad (3)$$

The APR usually displays a high selectivity; only trace amounts of hydrogenated by-products are produced [Equations (4)–(6)]:

$$CO\ (g) + 3\ H_2\ (g) \rightleftharpoons CH_4\ (g) + H_2O\ (g) \quad (4)$$

$$CO_2\ (g) + 4\ H_2\ (g) \rightleftharpoons CH_4\ (g) + 2\ H_2O\ (g) \quad (5)$$

$$2\,CO\,(g) + 5\,H_2\,(g) \rightleftharpoons C_2H_6\,(g) + 2\,H_2O\,(g) \quad (6)$$

With the careful selection of the catalyst and operating conditions, these hydrogenated by-products can be mostly avoided [24].

The methanol APR research has been mostly focused on finding suitable catalysts that promote the reforming reactions at temperatures as low as possible and inhibit undesired reactions [14,25]. Amongst noble (Pt, Ru) and non-noble (Ni, Cu) metals, Pt-based catalysts are the most used for methanol APR. Dumesic's group [17,18] studied the APR of different alcohols (e.g., methanol and ethylene glycol) with Pt supported on alumina (Pt/Al_2O_3). Specifically for methanol, their study was conducted at temperatures/pressures of 210 °C/2.24 MPa and 225 °C/2.96 MPa, on a Pt/Al_2O_3 catalyst with a Pt mass fraction of 0.59%, and with a feed aqueous solution with methanol mass fractions of 1%, 4%, and 10%. All the experiments were conducted with a feed flow rate of 0.30 mL/min, in order to keep the conversion below 3%. Their results showed that the reaction is weakly inhibited by hydrogen, which could be caused by the surface sites blocked by adsorbed hydrogen atoms and, in addition, by decreasing the surface concentrations of reactive intermediates formed from dehydrogenation of the methanol. They also found that the liquid-phase environment favors the water–gas shift reaction, mitigating the potential blocking of surface sites by adsorbed CO species. Since then, Pt-based catalysts for methanol APR have been improved, mostly concerning the catalyst support, where molybdenum carbide (MoC) [26], $NiAl_2O_4$ spinel [27], and zeolite [28] supports were reported. Ni-based catalysts have also been explored for the methanol APR as they favor the WGS reaction [14] and are inexpensive compared to noble metal-based catalysts. However, Ni-based catalysts suffer from lower stability (especially since they are more sensitive to oxidation under APR operating conditions) and lower hydrogen selectivity. These catalysts were studied mostly by Stekrova et al. [24] and Coronado et al. [13,22].

The present work studies the methanol APR reaction kinetics on Pt/Al_2O_3. The performance of the catalyst, with a nominal mass fraction of 5%, was investigated for the temperatures of 190 °C, 210 °C and 230 °C. The effect on the catalyst performance of the methanol mass fraction in the feed aqueous solution was studied as well, using a low value of 5% and a high value of 55%. The operating pressures used were above the bubble point of the corresponding feed stream, a minimum of 3.2 MPa for the low methanol mass fraction feed and a minimum of 5.2 MPa for the high methanol mass fraction feed. The performance of Pt/Al_2O_3 was characterized in terms of methanol conversion, hydrogen production rate, and hydrogen selectivity for a wide range of weight hourly space velocity (WHSV) values.

2. Results and Discussion

2.1. Physicochemical Characterization of the Catalyst

The H_2-TPR of a 5 wt.% Pt/Al_2O_3 sample is displayed in Figure 1; it exhibits the presence of a single sharp peak at ca. 300 °C, starting at ca. 250 °C and ending at ca. 325 °C. The presence of this single peak indicates that only one type of active metal is present in the catalyst. This TPR result is in good agreement with the XRD of the catalyst, showing only Pt and alumina—discussed in the following.

The information regarding the reducibility of Pt/Al_2O_3 was used to activate the catalyst in situ before the APR tests. Controlling the reduction temperature is important since the catalyst reduction (activation process) is an exothermic process that influences the catalyst's ability to perform the reforming reaction. Since small catalyst particle sizes are more prone to sintering, the reduction process was performed using diluted hydrogen at 300 °C.

XRD patterns of fresh and spent Pt/Al_2O_3 samples are shown in Figure 2. The spent catalyst was subjected to methanol APR for 7.5 h at 230 °C and 3.2 MPa using a 5 wt.% methanol aqueous solution supplied at 0.3 h^{-1} WHSV. Comparing fresh and spent catalysts, the XRD diffractogram of the spent sample shows that alumina support underwent phase change and Pt metal was sintered and leached.

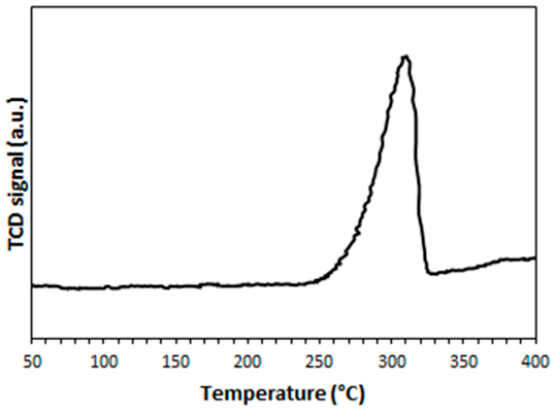

Figure 1. H_2-TPR of a 5 wt.% Pt/Al_2O_3 catalyst sample.

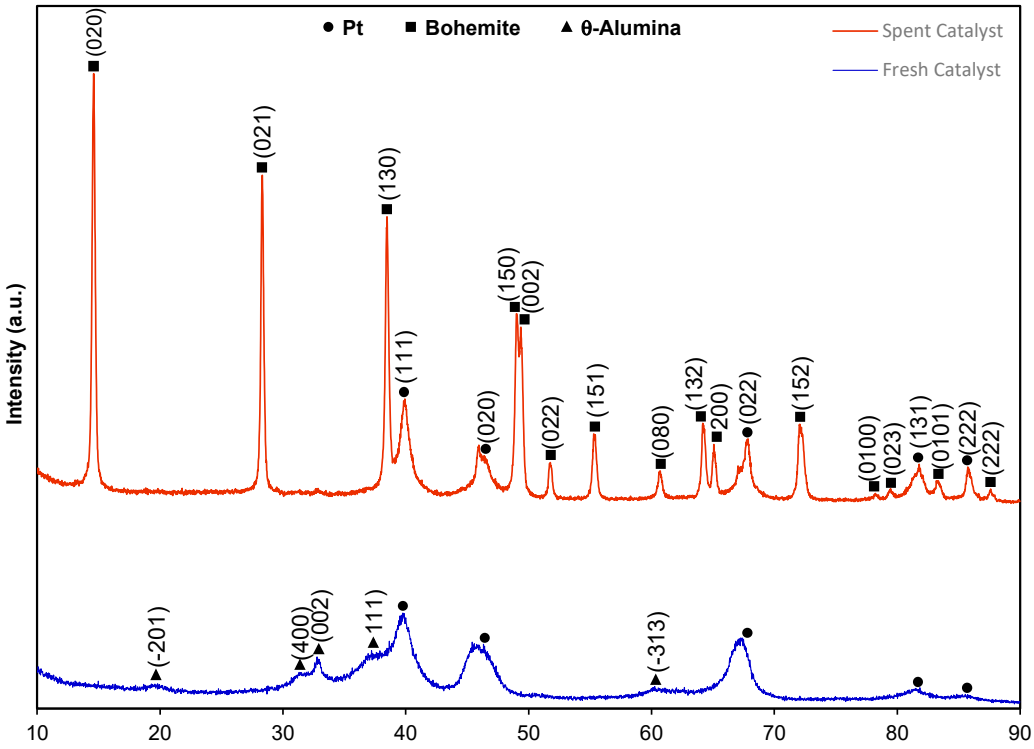

Figure 2. XRD diffractograms of fresh (blue line) and spent (red line) Pt/Al_2O_3 samples.

In both fresh and spent catalysts, characteristic Pt metallic peaks were detected at 2θ = 39.8°, 46.5°, and 67.8° (JCPDS 01-1190) [29]. However, these peaks are broader for the fresh catalyst compared to the spent catalyst. These could be due to poor crystallinity, overlapping with some of the alumina peaks [30], or smaller crystallite size. The calculated Pt crystallite size was estimated to be ca. 5 nm in the fresh catalyst sample, as shown in Table 1.

Table 1. Pt crystallize size and mass fraction for fresh and spent catalysts.

Pt Crystallite Size (nm)	Fresh Catalyst	Spent Catalyst
	5 (±2)	12 (±1)
Pt mass Fraction (%)	Fresh Catalyst	Spent Catalyst
	4.5 (±0.5)	3.1 (±1)

The spent catalyst has a Pt crystallite size of ca. 12 nm, indicating that Pt particles were sintered under the APR reaction conditions. The calculated amount of Pt in the fresh catalyst was ca. 4.5 wt.%, which is according to the value reported by the catalyst supplier. However, the spent catalyst showed approximately 3 wt.% of Pt mass, suggesting that leaching of Pt occurred during the APR reaction. Moreover, the spent catalysts showed peaks related to boehmite, while fresh catalyst only showed peaks for θ-alumina. The presence of this crystalline structure shows that alumina was transformed in boehmite, which is a thermodynamically more stable phase under high humidity levels, such as under APR reaction conditions [31].

The N_2 adsorption–desorption isotherm for the catalyst Pt/Al_2O_3 is shown in Figure 3 and the BET surface area, average pore size, and pore volume are listed in Table 2.

According to IUPAC classification, Pt/Al_2O_3 has a type (IV) isotherm which indicates the mesoporous structure of the catalyst with the pore size wider than 4 nm. The catalyst also showed an H3-type hysteresis loop. This is usually observed for the irregular pore system with agglomerated particles that are slit-shaped pores of irregular sizes or shapes [32].

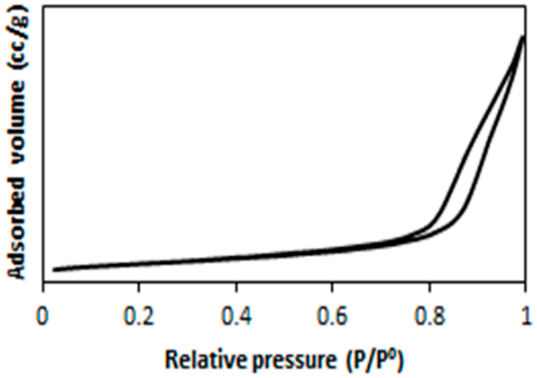

Figure 3. Nitrogen adsorption–desorption isotherm of Pt/Al_2O_3.

Table 2. Physicochemical properties of Pt/Al_2O_3.

Pt/Al_2O_3	BET Surface Area (m^2/g)	Pore Volume (cc/g)	Pore Diameter (nm)
	205.9	0.87	13.1

2.2. Kinetic Characterization

The methanol–water vapor pressure was obtained for temperatures of 190 °C, 210 °C, and 230 °C using the Aspen Technology software. The plot of the bubble pressure versus methanol mole fraction at the three different temperatures is shown in Figure 4. This plot is fundamental to assure that the kinetic characterization of methanol APR using the Pt/Al_2O_3 catalyst is properly carried out at all experimental conditions, i.e., with the feed methanol water mixture in liquid phase. As the methanol concentration increases, the required pressure to keep the mixture in a liquid state increases as well. In the literature, most experiments were performed using a 5 wt.% methanol aqueous solution, yet commercial HT-PEMFC systems that use methanol reformers for in situ hydrogen production typically run using 55 wt.% methanol aqueous solutions [33,34].

For a 55 wt.% methanol aqueous solution at 230 °C, it is required to keep the system at >5.1 MPa. On the other hand, for a 5 wt.% methanol aqueous solution, >3.1 MPa is sufficient for the same temperature.

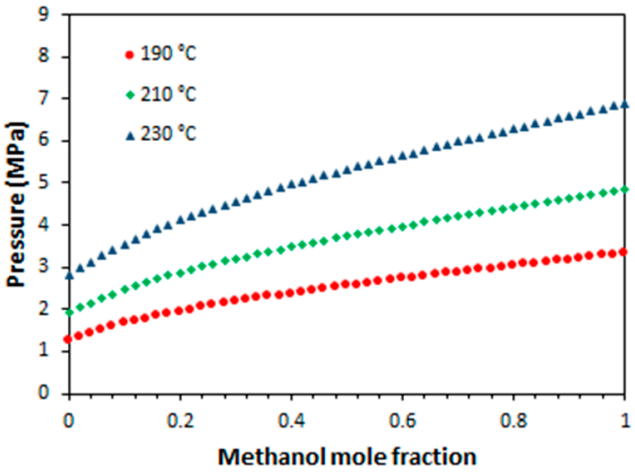

Figure 4. The bubble point pressures of binary methanol–water mixture for the different mole fractions of methanol for temperatures of 190 °C, 210 °C, and 230 °C were predicted using Aspen Technology.

2.2.1. Effect of Temperature

The effect of temperature on methanol APR conversion is depicted in Figure 5 for the temperatures 190 °C, 210 °C, and 230 °C. Thermodynamically and kinetically, either the desirable reforming or undesirable side reactions are favored by higher temperatures. On the other hand, a WGS reaction is disfavored at higher temperatures, though it is also favored kinetically with the temperature. An increase in the experimental methanol conversion was observed at higher temperatures. At the low temperature (190 °C), the methanol conversion does not go above 15%, even at a very low WHSV. Compared with the MSR, the performance of methanol APR at low temperatures is usually much lower; for example, even considering a different catalyst, at a WHSV of 1 h^{-1} and at 190 °C, the methanol conversion is ca. 75% for MSR in a Cu based catalyst [35], while for APR is less than 5% in the present work, Figure 5A. WHSV is defined as the weight of methanol in the feed stream normalized by the weight of the catalyst and time. Therefore, the methanol conversion should be similar for the same WHSV, independently of the methanol concentration, making negligible the effect of the methanol feed dilution on conversion. However, for the same WHSV, a change in the feed mass fraction of the aqueous methanol solution from 5 wt.% to 55 wt.% leads to an equivalent decrease of the feed flow rate for the same ratio, which may have some adverse influence in the conversion, for example, in the rate of adsorbed reaction products from the catalyst surface.

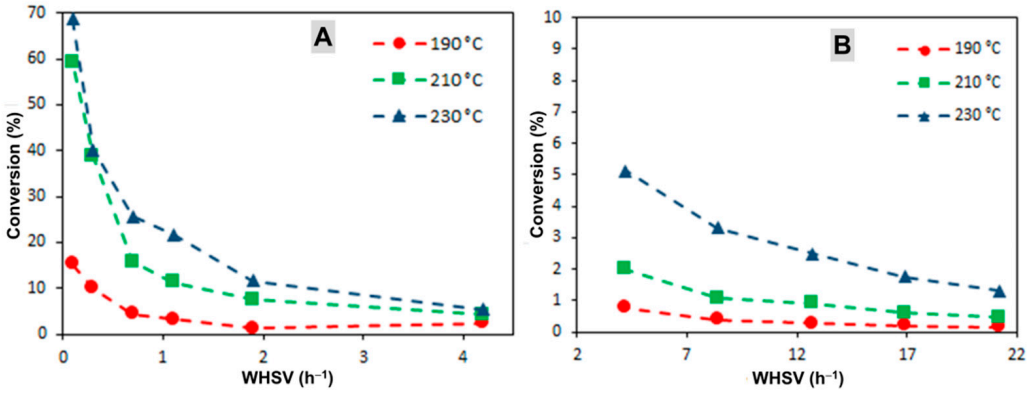

Figure 5. Methanol conversion in aqueous-phase reforming of (**A**) 5 wt.% and (**B**) 55 wt.% aqueous methanol solution over 5 wt.% Pt/Al_2O_3, N_2 co-feeding of 30 mL·min^{-1} and operating temperatures of 190 °C, 210 °C, and 230 °C as a function of WHSV. Operating pressure of 3.2 MPa (**A**) and 6.0 MPa (**B**). All values were obtained after achieving steady-state reaction conditions.

H_2 Production Rate

The APR has the potential to be integrated with an HT-PEMFC system due to its higher energy efficiency and simple recycling of unreacted reagents; this allows the APR to operate at conversions lower than 100% without significantly affecting the system efficiency. Moreover, HT-PEMFCs have a high tolerance to reforming contaminants (up to 3% [36,37]).

For 55 wt.% methanol feed aqueous solution, the maximum hydrogen production rate was ca. 500 $\mu mol \cdot min^{-1} \cdot g^{-1}_{cat}$. As depicted in Figure 6, the hydrogen production rate as a function of the WHSV peaks at WHSV $\approx$ 13 h^{-1}, especially for 210 °C and 230 °C, decreases slightly afterward. At higher methanol concentrations and for the same feed flow rate, the contact time between reactants and catalyst decreases, which adversely affects hydrogen production [17].

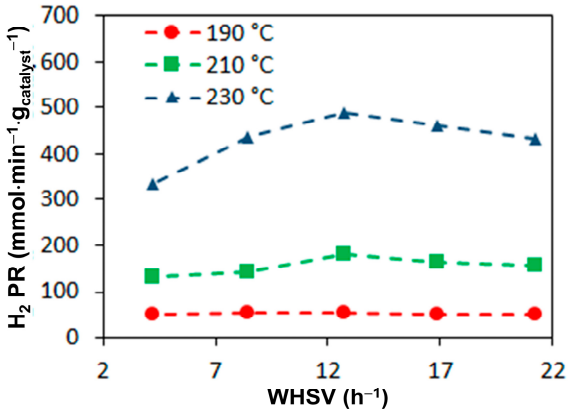

Figure 6. Hydrogen production rate in aqueous-phase reforming of 55 wt.% methanol feed aqueous solution over 5 wt.% Pt/Al_2O_3, N_2 co-feeding of 30 $mL \cdot min^{-1}$ and operating temperatures of 190 °C, 210 °C, and 230 °C at various WHSV. Operating pressure 6.0 MPa. All values were obtained after achieving steady-state reaction conditions.

By-Product Formation

Undesirable side reactions, such as methanation, are thermodynamically favored at higher temperatures and pressures. During the APR experiments, only by-products CH_4 and CO were detected at the GC analyzer. The low concentrations of by-products CH_4 and CO, inferior to 0.5%, as illustrated in the GC chromatogram of Figure 7, indicate high selectivity for the APR reaction.

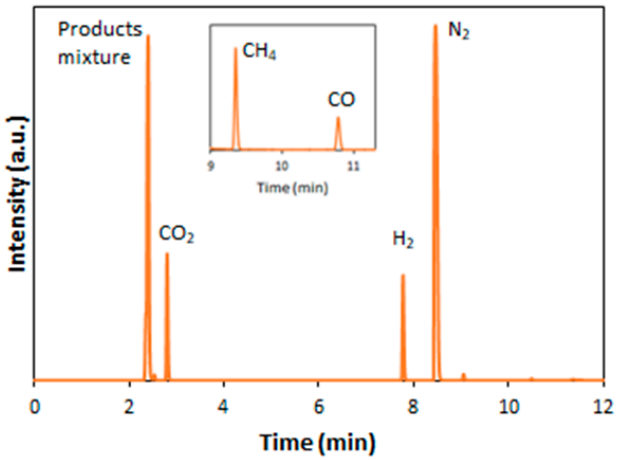

Figure 7. Gas chromatograph obtained from a 55 wt.% methanol aqueous-phase reforming on a 5 wt.% Pt/Al_2O_3 catalyst, with a N_2 co-feeding of 30 $mL \cdot min^{-1}$, operating conditions of 230 °C, 3.2 MPa, and 21.2 h^{-1} WHSV.

Figure 8 shows the CH_4 production rate as a function of WHSV for 190 °C, 210 °C, 230 °C, and 55 wt.% methanol aqueous solution. CH_4 production can follow two paths, via cleavage of C-O bonds of methanol followed by hydrogenation (by an acid-catalyzed pathway), or via methanation, which is the hydrogenation of carbon monoxide/carbon dioxide (COx) [17]. Both paths are independent of methanol conversion since hydrogen is required to perform the hydrogenation step; therefore, CH_4 formation occurs as a parallel reaction [17]. It is noticeable that the CH_4 formation increases with temperature (Figure 8), while it shows a more complex pattern with WHSV.

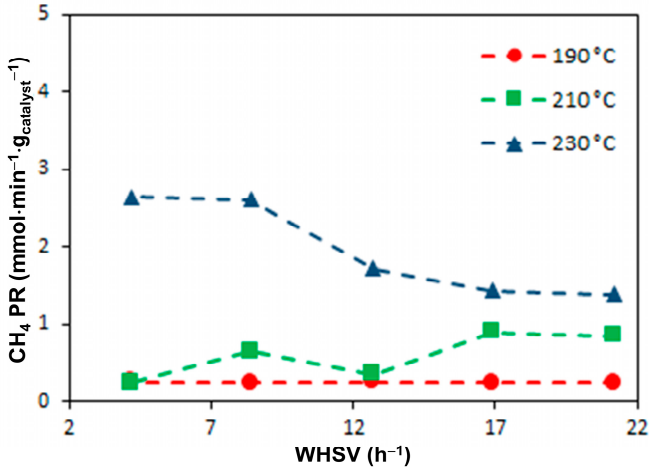

Figure 8. Methane production rate in aqueous-phase reforming fed with a 55 wt.% methanol aqueous solution, with an N_2 co-feeding of 30 mL·min^{-1}, operating at 190 °C, 210 °C, and 230 °C and at 6.0 MPa, as a function of the WHSV. All values were obtained after achieving steady-state reaction conditions.

2.2.2. Effect of Pressure

It is important to study the influence of the reaction pressure on APR performance since APR is a multiphase system with a reaction often occurring in a mass transfer-limited regime. Figure 9 shows the effects of operating pressure on methanol conversion at 230 °C. For a methanol feed mass fraction of 5 wt.%, the methanol conversion decreases from 25% at 3.2 MPa to 13% at 4.0 MPa (Figure 9A) and then it keeps more or less constant for higher pressures. For a methanol feed mass fraction of 55 wt.%, the methanol conversion is considerably lower and mostly constant with the reaction pressure, around 2% (Figure 9B). However, there is an apparent small increase in the conversion in the operating pressure region in the liquid phase. It should be emphasized, also, that a smaller conversion for a higher mass fraction of methanol in the feed stream does not necessarily lead to a lower hydrogen productivity, because of the higher amount of methanol feed to the reactor.

Performing the methanol-reforming reaction below the bubble point pressure (gaseous methanol reforming) for the methanol feed mass fraction of 55% did not yield conversions higher than those observed for methanol APR. This apparent discrepancy deserves further study in the future.

In multiphase systems, pressure affects density, bubble size distribution [38,39], and catalyst-wetting efficiency [40]. While the wetting efficiency increases with pressure [40], which is crucial for multiphase systems, increasing the operating pressure increases the hydrogen partial pressure, which negatively affects the reaction rate [17]. Hydrogen has very low solubility in water and methanol and diffuses slowly from the catalyst active site where it is formed to the bulk [18]; moreover, higher pressures reduce the bubble size, reducing the bubble disengaging rate. In this sense, the catalyst surface active sites are occupied for a longer time [17,18]. In addition, the hydrogen availability near an active site can promote the hydrogenation of intermediate species, leading to a loss in selectivity [18,41]. Since nitrogen (carrier gas) is also not soluble in the liquid reaction phase, it should leave the reactor mixed with hydrogen and CO_2, besides water and methanol vapors.

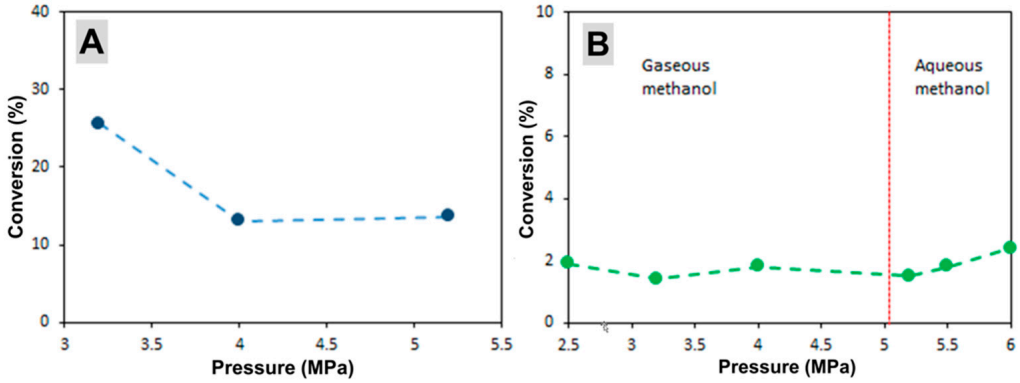

Figure 9. Methanol conversion as a function of pressure for (**A**) 5 wt.% and (**B**) 55 wt.% methanol aqueous solution over 5 wt.% Pt/Al_2O_3 catalyst. Operating temperature of 230 °C, WHSV of (**A**) 0.7 h^{-1} and (**B**) 12.7 h^{-1}. All values were obtained after achieving steady-state reaction conditions.

2.2.3. Selectivity of Methanol APR to Hydrogen

A high-methanol APR selectivity to hydrogen leads to a higher energy conversion efficiency from methanol to hydrogen and allows for directly feeding the reformate to an HT-PEMFC system. Apart from the nature of the catalyst (metal and support), the selectivity to hydrogen depends on the operating conditions [14]. Figure 10 shows the selectivity to hydrogen as a function of WHSV for different operating pressures.

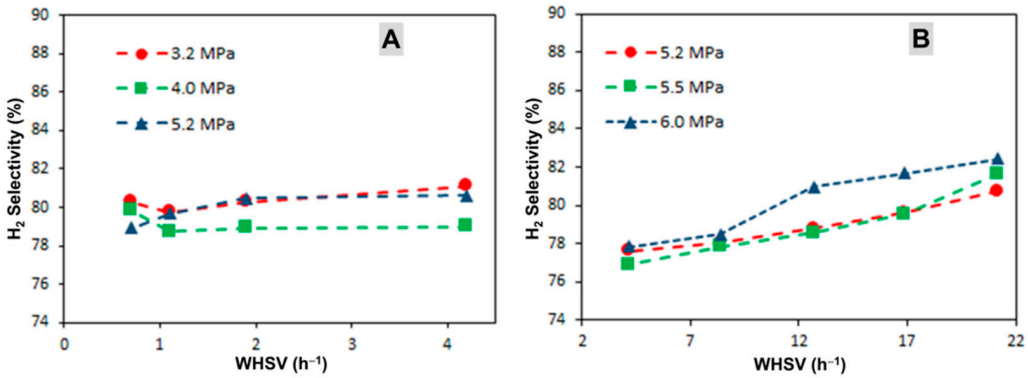

Figure 10. H_2 selectivity in aqueous-phase reforming of (**A**) 5 wt.% and (**B**) 55 wt.% methanol aqueous solution on a 5 wt.% Pt/Al_2O_3 catalyst, with a N_2 co-feeding of 30 mL·min^{-1} and at 230 °C, for various pressures and as a function of WHSV. All values were obtained after achieving steady-state reaction conditions.

For the methanol feed aqueous solution with a mass fraction of 5%, Figure 10A, the maximum change in the selectivity to hydrogen is of around 2%, either as a function of the operating pressure for a given WHSV, or as a function of the WHSV for a given operating pressure. For the methanol feed aqueous solution with a mass fraction of 50%, Figure 10B, the effect of the operating pressure for a given WHSV is also small; on the contrary, the influence of the WHSV for all three operating pressures is clearly more accentuated. For low-WHSV values (methanol mass fraction of 5%), the selectivity to hydrogen is mostly independent of the methanol conversion. Therefore, it may be concluded that hydrogen production over Pt/Al_2O_3 is not restricted by the hydrogenation of CO/CO_2. The selectivity to hydrogen is clearly above 75% for all experiments (Figure 10A,B), indicating that the H_2/CO_2 ratio for these experiments stayed above a factor of 3.

Apart from the nature of the catalyst (both metal and support) and operating conditions, the dependence of the selectivity to hydrogen with the reactor design has also been studied. It was reported that, by using a microchannel reactor instead of a fixed-bed reactor, the selectivity to hydrogen becomes higher by a factor of two, regardless of the feedstock

conversion [42]. The selectivity to hydrogen in a microchannel reactor should increase because of a better catalyst wettability, making the mass transfer of hydrogen from the catalyst site to the gas phase faster [42]. Table 3 below summarizes the APR performance results (in terms of selectivity to CO_2, CO, CH_4) at various WHSVs and operating pressures.

Table 3. Selectivity of the CO_2, CH_4, and CO in methanol APR experiments at various operating pressures and for different WHSVs.

Product	Methanol Concentration	WHSV (h^{-1})	Selectivity (%)				
			3.2 MPa	4.0 MPa	5.2 MPa	5.5 MPa	6.0 MPa
CO_2	5 wt.%	0.7	19.7	20.8	19.1		
		1.1	20.2	21	19.4		
		1.9	19.4	21.2	20.2		
		4.2	18.5	20	20.9		
	55 wt.%	4.2			21.6	21.6	21.5
		8.4			21.3	21.0	21
		12.7			20.7	20.5	18.7
		16.9			19.9	19.6	18
		21.2			18.8	17.7	17.2
CH_4	5 wt.%	0.7	0.1	0.1	0.2		
		1.1	n/a	0.08	0.1		
		1.9	0.2	0.05	0.1		
		4.2	0.3	0.19	0.1		
	55 wt.%	4.2			0.3	0.9	0.6
		8.4			0.3	0.9	0.4
		12.7			0.3	0.7	0.3
		16.9			0.4	0.6	0.2
		21.2			0.4	0.5	0.2
CO	5 wt.%	0.7	0.05	0.02	0.02		
		1.1	0.07		0.05		
		1.9	0.04	0.01	0.05		
		4.2	0.01	0.03	0.05		
	55 wt.%	4.2			0.1	0.6	0.05
		8.4			0.1	0.2	0.04
		12.7			0.1	0.2	0.04
		16.9			0.1	0.2	0.1
		21.2			0.1	0.1	0.1

Long-Term Stability Test

The long-term stability of methanol APR was performed to study the effects on catalyst performance and methanol conversion. Figure 11 shows the methanol conversion as a function of time for a 5 wt.% methanol feed aqueous solution. Steady-state performance was achieved for >7 h.

The catalytic activity increased at the beginning and then slowly decreased until reaching a steady state. The decrease in the catalytic activity (methanol conversion) may be assigned to the phase change of the support alumina into boehmite, metal phase sintering, and Pt leaching, as discussed before.

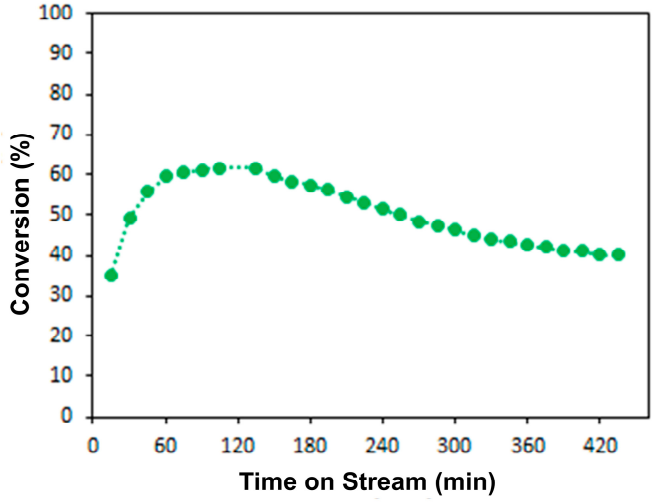

Figure 11. Methanol conversion as a function of time on stream for 5 wt.% methanol aqueous solution over 5 wt.% Pt/Al_2O_3 at 230 °C and 3.3 MPa and 0.3 h^{-1} WHSV.

2.3. Methanol Steam Reforming Versus Aqueous-Phase Reforming

Methanol has the potential to make hydrogen dispatchable, which is critical for the development of the so-called hydrogen economy. MSR is an established pathway to produce in situ hydrogen, with extensive research performed on catalysts, reactors, and purification of the produced hydrogen. Most MSR employs Cu-based catalysts due to their low cost, high hydrogen yield, and low CO production [43–45]. Methanol APR, on the other hand, is a relatively new technology where the catalyst development is still underdeveloped. Pt-based catalysts are widely used in APR due to their stability and moderate performance [25,43]. Figure 12 illustrates the interest in these two reforming processes measured by the number of publications during the last two decades.

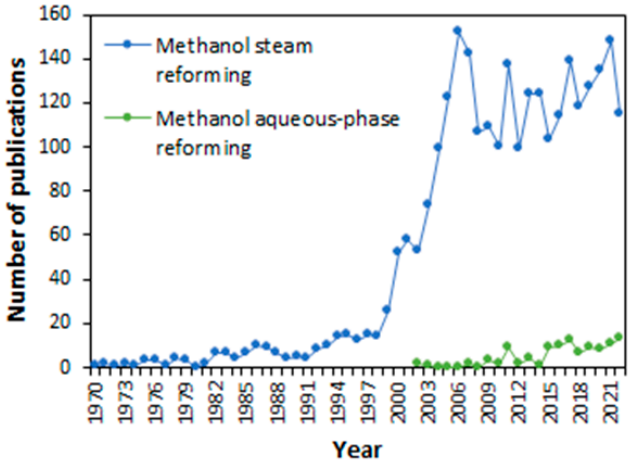

Figure 12. The number of scientific publications on methanol steam reforming and methanol aqueous-phase reforming (information retrieved from Scopus database).

Methanol APR in Pt/Al_2O_3 suffers from low stability and displays low yields, which reduces its potential interest to industrial applications.

However, the possibility of running the reforming reaction in the liquid phase and then saving the vaporization energy is still driving the research community for developing better-performing catalysts. To use HT-PEMFCs in mobile applications, which require high power output, there are certain operating condition requirements for methanol reforming that should be fulfilled: compact reforming systems, operation close to the stoichiometric

concentration of methanol–water and at a temperature which allows its thermal integration with an HT-PEMFC [46–48].

At around 100 °C, the methanol steam reforming (MSR) produces just hydrogen and CO_2; the CO concentration is negligible. However, above 150 °C, there is the onset production of CO whose concentration in the product stream increases with the temperature [35,49]. Yu et al. [49] reported that the CO concentration in the product stream was 511 ppm, when the MSR reactor was run at 190 °C, for a contact time (W/F) of 180 $kg_{cat}\cdot(mol\cdot s^{-1})^{-1}$ (almost full conversion of the methanol). For 230 °C, it was 2184 ppm. Ribeirinha et al. [35] reported a CO concentration of 600 ppm at the product stream when the MSR reactor was run at 180 °C, on a $CuO/ZnO/Ga_2O_3$ catalyst, and for a W/F of 60 $kg_{cat}\cdot(mol\cdot s^{-1})^{-1}$ (ca. 80% of methanol conversion).

From the present work, we report CO production between 100 ppm (190 °C) and 1990 ppm (230 °C) [647.1 $kg_{cat}\cdot(mol\cdot s^{-1)-1}$–5.5 $kg_{cat}\cdot(mol\cdot s^{-1})^{-1}$] using a commercial Pt/Al_2O_3. Although the CO concentration is lower for the methanol APR at lower temperatures, as the temperature increases, the CO concentration in the product becomes similar for both types of methanol reforming. However, it should be emphasized that the CO concentration also depends on the reactor used for the reforming.

2.4. Perspectives

Catalyst development remains a primary focus of research for methanol APR; Pt-based catalysts are the best-performing catalysts. However, as seen in this work, support plays an equally important role in the catalyst performance. Therefore, various supports other than metal oxides should be assessed to improve the activity and stability of the catalyst. Furthermore, the long-term stability of the catalyst should be studied to better understand the catalyst deactivation under APR conditions.

In addition to the catalyst development, the mass transfer limitation of the reaction products from the active sites poses one of the greatest challenges to overcome. Nitrogen co-feeding has been employed to mitigate this issue. However, the dilution of hydrogen due to the co-feeding of nitrogen can adversely affect the performance of HT-PEMFCs during reformer/fuel cell integration. Therefore, novel reactor designs should be proposed and studied to minimize the mass transport limitation to allow higher hydrogen productivity at lower temperatures by effectively removing reaction products from the active sites. Following, the use of a membrane reactor, selective to hydrogen, may be considered as an alternative to a conventional fixed-bed reactor. Reactors such as coated microchannel reactors [50] and membrane reactors facilitate the effective removal of hydrogen from the reaction medium; for example, D´Angelo et al. [51] have reported that using a carbon-coated ceramic membrane reactor yielded 2.5 times higher hydrogen than a fixed-bed reactor for APR of sorbitol.

3. Experiment

3.1. Materials

Pt/Al_2O_3 catalyst (5 wt.% Pt loading) supplied by Sigma-Aldrich (St. Louis, MO, USA) in powder form was used without further modification.

3.2. Physicochemical Characterization

Hydrogen-temperature-programmed reduction (H_2-TPR) and X-ray diffraction (XRD) were used to determine the physicochemical properties of the Pt/Al_2O_3 catalyst. Multipoint Brunauer–Emmett–Teller (BET) provided information regarding the surface area and pore size of the catalyst. XRD patterns were recorded at room temperature, using a Panalytical MPD diffractometer equipped (Almelo, The Netherlands) with an X′ Celerator detector and secondary monochromator in Bragg–Brentano geometry. $CuK\alpha_{1,2}$ radiation, λ_1 = 1.5406 Å, λ_2 = 1.5444 Å, a step size of 0.017° and 100 s/step were used. Rietveld refinements were performed using the software PowderCell 2.4 to calculate Pt crystallite size.

The mass fraction of Pt in the catalyst was estimated in a Thermo Scientific iCAP 7400 ICP-OES Duo instrument (Boston, MA, USA), coupled with an ASX-520 autosampler.

A ChemBET Pulsar TPR/TPD instrument (Anton Paar, Ashland, VA, USA) equipped with a TCD was used to perform H_2-TPR experiments. Approximately 25 mg of catalyst was placed in a U-shaped quartz tube reactor and held in place with quartz wool. The sample was heated from 50 °C to 450 °C at a heating rate of 5 °C·min^{-1} under constant H_2/Ar (1:9) flow. Multipoint BET surface measurements were performed on a Quantachrome Autosorb AS-1 instrument (Anton Paar, Ashland, VA, USA) at −196 °C. Prior to the analysis, the samples were outgassed in vacuum at 200 °C for 4 h.

3.3. Reaction Kinetic Experimental Setup

A cylindrical stainless-steel FBR (70 mm L × 7 mm ID) was used to conduct the methanol APR experiments. A 700 mg catalyst sample and an equal amount of glass beads were mixed and loaded into the midsection of the reactor. Glass wool and wire mesh were inserted at both ends of the reactor to avoid dragging the catalyst and glass beads with the product's and reactant's flow. The reactor was placed vertically inside a temperature-controlled oven. Figure 13 shows a schematic representation of the laboratory scale set-up used for this work.

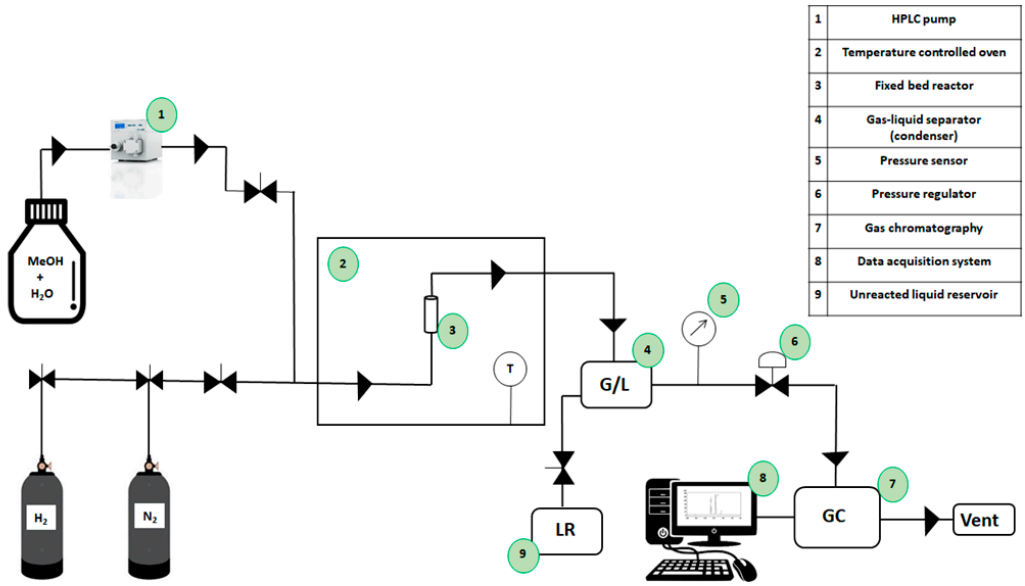

Figure 13. Schematic representation of methanol aqueous-phase reforming experimental set-up.

Before the methanol APR tests, Pt/Al_2O_3 was reduced in situ at 300 °C for 2 h in a flowing H_2/N_2 (1:1) atmosphere. Afterward, the reactor was purged with N_2 gas (50 mL·min^{-1}) for 30 min to remove the adsorbed hydrogen. For this study, methanol APR activity tests were performed at temperatures of 190 °C, 210 °C, and 230 °C, and pressures of 3.2 MPa, 4.0 MPa, 5.2 MPa, 5.5 MPa, and 6.0 MPa with N_2 co-feeding (sweep gas) at 30 mL·min^{-1}. Two different methanol aqueous solutions, 5 wt.% and 55 wt.% of methanol, were tested under the above-mentioned experimental conditions. To keep the reaction in the liquid phase, binary equilibrium plots for the methanol–water mixture were simulated using Aspen Plus (Aspen Technology Software V37.0) (Wilson-Ideal equation property package). These phase diagrams were obtained for the different methanol–water mixtures at various operating temperatures.

The methanol aqueous solution was fed upwards using an HPLC pump (KNAUER Smartline Manager 5050, Berlin, Germany) with a WHSV between 0.1 h^{-1} and 21.2 h^{-1}. The output stream was cooled down in a condenser at ca. 0 °C to separate the liquid-phase and gaseous-phase streams. The concentration of the gaseous-phase components was measured with online gas chromatography (GC) (Shimadzu GC 2010 Plus, Kyoto, Japan) equipped with two columns, Pora-Plot Q (Agilent, Santa Clara, CA, USA) and HP-Molesieve (Agilent),

and a barrier ionization discharge detector (BID, Shimadzu, Kyoto, Japon). The catalytic activity was evaluated in terms of methanol conversion (%) (Equation (7)), H_2 production rate ($\mu mol \cdot min^{-1} \cdot g_{catalyst}{}^{-1}$) (Equation (8)), CH_4 production rate ($\mu mol \cdot min^{-1} \cdot g_{catalyst}{}^{-1}$) (Equation (9)), and H_2 selectivity (%) (Equation (10)).

$$\text{Methanol conversion } (\%) = \left(\frac{n\text{MeOH}_{\text{in}} - n\text{MeOH}_{\text{out}}}{n\text{MeOH}_{\text{in}}}\right) \times 100 \quad (7)$$

$$\text{H}_2 \text{ production rate } (\mu mol \cdot min^{-1} \cdot g_{catalyst}{}^{-1}) = \frac{n(\text{H}_2)}{m_{catalyst}} \quad (8)$$

$$\text{CH}_4 \text{ production rate } (\mu mol \cdot min^{-1} \cdot g_{catalyst}{}^{-1}) = \frac{n(\text{CH}_4)}{m_{catalyst}} \quad (9)$$

$$\text{Selectivity }_{\text{Hydrogen}} (\%) = \frac{n(\text{H}_2)}{\sum GasProducts_{\text{out}}} \times 100 \quad (10)$$

Herein, n denotes the molar flow rate, MeOH_{in} means methanol in the inlet flow, MeOH_{out} means methanol in the outlet flow, and $m_{catalyst}$ is the mass of the catalyst in grams. All values were obtained after achieving steady-state reaction conditions.

4. Conclusions

This work studies the effects of various operating conditions in methanol APR using a commercial Pt/Al_2O_3. As expected, increasing operating temperature and residence time were beneficial for APR performance. Methanol conversion was, however, below 5% while using 55 wt.% methanol feedstock at 190 °C. Despite the low methanol conversion obtained using high-methanol concentration feed (55 wt.%), the hydrogen production rate that was achieved was high. As the operating pressure was increased beyond bubble point pressure, methanol conversion dropped drastically due to the increase in mass transfer limitations. However, increasing the operating pressure did not affect the hydrogen selectivity. It was also concluded that alkane formation in APR also occurs due to parallel pathway reactions in addition to hydrogenation of CO/CO_2 but at a minute level. Slight deactivation was observed using 5 wt.% methanol feedstock after the long-term stability experiment due to the alumina phase changing into boehmite and Pt sintering and leaching.

Nonetheless, APR has come up to be an encouraging technology for hydrogen production. Several shortcomings of APR have been listed that should be researched to achieve higher hydrogen production and increased catalyst stability.

Author Contributions: The contributions of the authors for the manuscript are the following: conceptualization, A.M.; methodology, A.M., J.S., P.L. and P.R.; investigation, P.L.; resources, A.M.; writing—original draft preparation, P.L.; writing—review and editing, A.M., J.S., P.R., W.H. and J.T.; supervision, A.M., J.S. and P.R.; project administration, A.M. and P.R.; funding acquisition, W.H. and J.T. All authors have read and agreed to the published version of the manuscript.

Funding: This work was supported by: (i) Fuel Cells and Hydrogen 2 Joint Undertaking (JU) under grant agreement number 875081. The JU receives support from the European Union's Horizon 2020 research and innovation programme and Finland, Denmark, Sweden, Portugal; (ii) H2Driven Green Agenda, number C644923817-00000037, investment project number 50, financed by the Recovery and Resilience Plan (PRR) and by European Union—Next Generation EU; and (iii) LEPABE, UIDB/00511/2020 (DOI: 10.54499/UIDB/00511/2020) and UIDP/00511/2020 (DOI: 10.54499/UIDP/00511/2020) and ALiCE, LA/P/0045/2020 (DOI: 10.54499/LA/P/0045/2020).

Data Availability Statement: The data presented in this study are available on request from the corresponding author.

Conflicts of Interest: Authors Werneri Huhtinen and Johan Tallgren were employed by the company VTT Technical Research Centre of Finland Ltd. The remaining authors declare that the research was conducted in the absence of any commercial or financial relationships that could be construed as a potential conflict of interest.

Abbreviations

APR	Aqueous-phase reforming
FBR	Fixed-bed reactor
GC	Gas chromatography
HPLC	High-performance liquid chromatography
MSR	Methanol steam reforming
PR	Production rate
TPD	Temperature-programmed desorption
TPR	Temperature-programmed reduction
WGS	Water–gas shift
WHSV	Weight hourly space velocity
XRD	X-ray diffraction

References

1. Dillman, K.; Heinonen, J. A 'just' hydrogen economy: A normative energy justice assessment of the hydrogen economy. *Renew. Sustain. Energy Rev.* **2022**, *167*, 112648. [CrossRef]
2. Kar, S.K.; Harichandan, S.; Roy, B. Bibliometric analysis of the research on hydrogen economy: An analysis of current findings and roadmap ahead. *Int. J. Hydrogen Energy* **2022**, *47*, 10803–10824. [CrossRef]
3. Nastasi, B. Power to Gas and Hydrogen applications to energy systems at different scales—Building, District and National level. *Int. J. Hydrogen Energy* **2019**, *19*, 9485. [CrossRef]
4. van der Spek, M.; Banet, C.; Bauer, C.; Gabrielli, P.; Goldthorpe, W.; Mazzotti, M.; Munkejord, S.T.; Røkke, N.A.; Shah, N.; Sunny, N.; et al. Perspective on the hydrogen economy as a pathway to reach net-zero CO_2 emissions in Europe. *Energy Environ. Sci.* **2022**, *15*, 1034–1077. [CrossRef]
5. Jain, I. Hydrogen the fuel for 21st century. *Int. J. Hydrogen Energy* **2009**, *34*, 7368–7378. [CrossRef]
6. Tarhan, C.; Çil, M.A. A study on hydrogen, the clean energy of the future: Hydrogen storage methods. *J. Energy Storage* **2021**, *40*, 102676. [CrossRef]
7. Muellerlanger, F.; Tzimas, E.; Kaltschmitt, M.; Peteves, S. Techno-economic assessment of hydrogen production processes for the hydrogen economy for the short and medium term. *Int. J. Hydrogen Energy* **2007**, *32*, 3797–3810. [CrossRef]
8. Dawood, F.; Anda, M.; Shafiullah, G.M. Hydrogen Production for Energy: An Overview. *Int. J. Hydrogen Energy* **2020**, *45*, 3847–3869. [CrossRef]
9. Ajanovic, A.; Haas, R. Prospects and impediments for hydrogen and fuel cell vehicles in the transport sector. *Int. J. Hydrogen Energy* **2020**, *46*, 10049–10058. [CrossRef]
10. Griffiths, S.; Sovacool, B.K.; Kim, J.; Bazilian, M.; Uratani, J.M. Industrial decarbonization via hydrogen: A critical and systematic review of developments, socio-technical systems and policy options. *Energy Res. Soc. Sci.* **2021**, *80*, 102208. [CrossRef]
11. Goma, D.; Delgado, J.J.; Lefferts, L.; Faria, J.; Calvino, J.J.; Cauqui, M. Catalytic Performance of $Ni/CeO_2/X\text{-}ZrO_2$ (X = Ca, Y) Catalysts in the Aqueous-Phase Reforming of Methanol. *Nanomaterials* **2019**, *9*, 1582. [CrossRef] [PubMed]
12. Kubacka, A.; Fernández-García, M.; Martínez-Arias, A. Catalytic hydrogen production through WGS or steam reforming of alcohols over Cu, Ni and Co catalysts. *Appl. Catal. A Gen.* **2016**, *518*, 2–17. [CrossRef]
13. Coronado, I.; Stekrova, M.; Moreno, L.G.; Reinikainen, M.; Simell, P.; Karinen, R.; Lehtonen, J. Aqueous-phase reforming of methanol over nickel-based catalysts for hydrogen production. *Biomass Bioenergy* **2017**, *106*, 29–37. [CrossRef]
14. Davda, R.; Shabaker, J.; Huber, G.; Cortright, R.; Dumesic, J. A review of catalytic issues and process conditions for renewable hydrogen and alkanes by aqueous-phase reforming of oxygenated hydrocarbons over supported metal catalysts. *Appl. Catal. B Environ.* **2005**, *56*, 171–186. [CrossRef]
15. Martín, M.; Grossmann, I.E. Optimal Simultaneous Production of Hydrogen and Liquid Fuels from Glycerol: Integrating the Use of Biodiesel Byproducts. *Ind. Eng. Chem. Res.* **2014**, *53*, 7730–7745. [CrossRef]
16. Cortright, R.D.; Davda, R.R.; Dumesic, J.A. Hydrogen from catalytic reforming of biomass-derived hydrocarbons in liquid water. *Mater. Sustain. Energy* **2010**, *418*, 289–292. [CrossRef]
17. Shabaker, J.; Davda, R.; Huber, G.; Cortright, R.; Dumesic, J. Aqueous-phase reforming of methanol and ethylene glycol over alumina-supported platinum catalysts. *J. Catal.* **2003**, *215*, 344–352. [CrossRef]
18. Shabaker, J.W.; Dumesic, J.A. Kinetics of Aqueous-Phase Reforming of Oxygenated Hydrocarbons: Pt/Al_2O_3 and Sn-Modified Ni Catalysts. *Ind. Eng. Chem. Res.* **2004**, *43*, 3105–3112. [CrossRef]
19. Shabaker, J.; Huber, G.; Dumesic, J. Aqueous-phase reforming of oxygenated hydrocarbons over Sn-modified Ni catalysts. *J. Catal.* **2004**, *222*, 180–191. [CrossRef]
20. Pipitone, G.; Zoppi, G.; Pirone, R.; Bensaid, S. A critical review on catalyst design for aqueous phase reforming. *Int. J. Hydrogen Energy* **2022**, *47*, 151–180. [CrossRef]
21. Davda, R.; Shabaker, J.; Huber, G.; Cortright, R.; Dumesic, J. Aqueous-phase reforming of ethylene glycol on silica-supported metal catalysts. *Appl. Catal. B Environ.* **2003**, *43*, 13–26. [CrossRef]

22. Coronado, I.; Pitínová, M.; Karinen, R.; Reinikainen, M.; Puurunen, R.L.; Lehtonen, J. Aqueous-phase reforming of Fischer-Tropsch alcohols over nickel-based catalysts to produce hydrogen: Product distribution and reaction pathways. *Appl. Catal. A Gen.* **2018**, *567*, 112–121. [CrossRef]
23. Kotowicz, J.; Brzęczek, M. Methods to increase the efficiency of production and purification installations of renewable methanol. *Renew. Energy* **2021**, *177*, 568–583. [CrossRef]
24. Stekrova, M.; Rinta-Paavola, A.; Karinen, R. Hydrogen production via aqueous-phase reforming of methanol over nickel modified Ce, Zr and La oxide supports. *Catal. Today* **2018**, *304*, 143–152. [CrossRef]
25. Coronado, I.; Stekrova, M.; Reinikainen, M.; Simell, P.; Lefferts, L.; Lehtonen, J. A review of catalytic aqueous-phase reforming of oxygenated hydrocarbons derived from biorefinery water fractions. *Int. J. Hydrogen Energy* **2016**, *41*, 11003–11032. [CrossRef]
26. Lin, L.; Zhou, W.; Gao, R.; Yao, S.; Zhang, X.; Xu, W.; Zheng, S.; Jiang, Z.; Yu, Q.; Li, Y.-W.; et al. Low-temperature hydrogen production from water and methanol using Pt/α-MoC catalysts. *Nature* **2017**, *544*, 80–83. [CrossRef] [PubMed]
27. Li, D.; Li, Y.; Liu, X.; Guo, Y.; Pao, C.-W.; Chen, J.-L.; Hu, Y.; Wang, Y. $NiAl_2O_4$ Spinel Supported Pt Catalyst: High Performance and Origin in Aqueous-Phase Reforming of Methanol. *ACS Catal.* **2019**, *9*, 9671–9682. [CrossRef]
28. Tang, Z.; Monroe, J.; Dong, J.; Nenoff, T.; Weinkauf, D. Platinum-Loaded NaY Zeolite for Aqueous-Phase Reforming of Methanol and Ethanol to Hydrogen. *Ind. Eng. Chem. Res.* **2009**, *48*, 2728–2733. [CrossRef]
29. El Doukkali, M.; Iriondo, A.; Cambra, J.; Gandarias, I.; Jalowiecki-Duhamel, L.; Dumeignil, F.; Arias, P. Deactivation study of the Pt and/or Ni-based γ-Al_2O_3 catalysts used in the aqueous phase reforming of glycerol for H_2 production. *Appl. Catal. A Gen.* **2014**, *472*, 80–91. [CrossRef]
30. Zambare, R.S.; Vaidya, P.D. Aqueous-phase reforming of model compounds of wet biomass to hydrogen on alumina-supported metal catalysts. *Int. J. Chem. Kinet.* **2024**, *56*, 265–278. [CrossRef]
31. Pipitone, G.; Zoppi, G.; Ansaloni, S.; Bocchini, S.; Deorsola, F.A.; Pirone, R.; Bensaid, S. Towards the sustainable hydrogen production by catalytic conversion of C-laden biorefinery aqueous streams. *Chem. Eng. J.* **2019**, *377*, 120677. [CrossRef]
32. Thommes, M.; Kaneko, K.; Neimark, A.V.; Olivier, J.P.; Rodriguez-Reinoso, F.; Rouquerol, J.; Sing, K.S.W. Physisorption of gases, with special reference to the evaluation of surface area and pore size distribution (IUPAC Technical Report). *Pure Appl. Chem.* **2015**, *87*, 1051–1069. [CrossRef]
33. Justesen, K.K.; Andreasen, S.J.; Pasupathi, S.; Pollet, B.G. Modeling and control of the output current of a Reformed Methanol Fuel Cell system. *Int. J. Hydrogen Energy* **2015**, *40*, 16521–16531. [CrossRef]
34. Andreasen, S.J.; Kær, S.K.; Sahlin, S. Control and experimental characterization of a methanol reformer for a 350 W high temperature polymer electrolyte membrane fuel cell system. *Int. J. Hydrogen Energy* **2013**, *38*, 1676–1684. [CrossRef]
35. Ribeirinha, P.; Mateos-Pedrero, C.; Boaventura, M.; Sousa, J.; Mendes, A. CuO/ZnO/Ga2O3 catalyst for low temperature MSR reaction: Synthesis, characterization and kinetic model. *Appl. Catal. B Environ.* **2018**, *221*, 371–379. [CrossRef]
36. Ribeirinha, P.; Abdollahzadeh, M.; Pereira, A.; Relvas, F.; Boaventura, M.; Mendes, A. High temperature PEM fuel cell integrated with a cellular membrane methanol steam reformer: Experimental and modelling. *Appl. Energy* **2018**, *215*, 659–669. [CrossRef]
37. Li, Q.; He, R.; Gao, J.-A.; Jensen, J.O.; Bjerrum, N.J. The CO Poisoning Effect in PEMFCs Operational at Temperatures up to 200 °C. *J. Electrochem. Soc.* **2003**, *150*, A1599. [CrossRef]
38. Iliuta, I. Performance of Fixed Bed Reactors with Two-Phase Upflow and Downflow. *J. Chem. Technol. Biotechnol.* **1997**, *68*, 47–56. [CrossRef]
39. Iliuta, I.; Thyrion, F. Flow regimes, liquid holdups and two-phase pressure drop for two-phase cocurrent downflow and upflow through packed beds: Air/Newtonian and non-Newtonian liquid systems. *Chem. Eng. Sci.* **1997**, *52*, 4045–4053. [CrossRef]
40. Dudukovic, M.P.; Larachi, F.; Mills, P.L. Multiphase reactors—Revisited. *Chem. Eng. Sci.* **1999**, *54*, 1975–1995. [CrossRef]
41. García, L.; Valiente, A.; Oliva, M.; Ruiz, J.; Arauzo, J.; García, L.; Valiente, A.; Oliva, M.; Ruiz, J.; Arauzo, J. Influence of operating variables on the aqueous-phase reforming of glycerol over a Ni/Al coprecipitated catalyst. *Int. J. Hydrogen Energy* **2018**, *43*, 20392–20407. [CrossRef]
42. D'Angelo, M.F.N.; Ordomsky, V.; van der Schaaf, J.; Schouten, J.C.; Nijhuis, T.A. Aqueous phase reforming in a microchannel reactor: The effect of mass transfer on hydrogen selectivity. *Catal. Sci. Technol.* **2013**, *3*, 2834–2842. [CrossRef]
43. Lakhtaria, P.; Ribeirinha, P.; Huhtinen, W.; Viik, S.; Sousa, J.; Mendes, A. Hydrogen production via aqueous-phase reforming for high-temperature proton exchange membrane fuel cells–A review. *Open Res. Eur.* **2022**, *23*, 81. [CrossRef] [PubMed]
44. Iulianelli, A.; Ribeirinha, P.; Mendes, A.; Basile, A. Methanol steam reforming for hydrogen generation via conventional and membrane reactors: A review. *Renew. Sustain. Energy Rev.* **2014**, *29*, 355–368. [CrossRef]
45. Palo, D.R.; Dagle, R.A.; Holladay, J.D. Methanol Steam Reforming for Hydrogen Production. *Chem. Rev.* **2007**, *107*, 3992–4021. [CrossRef]
46. Brett, D.J.L.; Brandon, N.P.; Hawkes, A.D.; Staffell, I. Fuel cell systems for small and micro combined heat and power (CHP) applications. In *Small and Micro Combined Heat and Power (CHP) Systems—Advanced Design, Performance, Materials and Applications*; Beith, R., Ed.; Woodhead Publishing Limited: Cambridge, UK, 2011; pp. 233–261. [CrossRef]
47. Ribeirinha, P.; Alves, I.; Vázquez, F.V.; Schuller, G.; Boaventura, M.; Mendes, A. Heat integration of methanol steam reformer with a high-temperature polymeric electrolyte membrane fuel cell. *Energy* **2017**, *120*, 468–477. [CrossRef]
48. Avgouropoulos, G.; Paxinou, A.; Neophytides, S. In situ hydrogen utilization in an internal reforming methanol fuel cell. *Int. J. Hydrogen Energy* **2014**, *39*, 18103–18108. [CrossRef]

49. Yu, K.M.K.; Tong, W.; West, A.; Cheung, K.; Li, T.; Smith, G.; Guo, Y.; Tsang, S.C.E. Non-syngas direct steam reforming of methanol to hydrogen and carbon dioxide at low temperature. *Nat. Commun.* **2012**, *3*, 1230. [CrossRef]
50. D'Angelo, M.F.N.; Ordomsky, V.; Paunovic, V.; van der Schaaf, J.; Schouten, J.C.; Nijhuis, T.A. Hydrogen Production through Aqueous-Phase Reforming of Ethylene Glycol in a Washcoated Microchannel. *ChemSusChem* **2013**, *6*, 1708–1716. [CrossRef]
51. D'Angelo, M.F.N.; Ordomsky, V.; Schouten, J.C.; van der Schaaf, J.; Nijhuis, T.A. Carbon-Coated Ceramic Membrane Reactor for the Production of Hydrogen by Aqueous-Phase Reforming of Sorbitol. *ChemSusChem* **2014**, *7*, 2007–2015. [CrossRef]